PHYSICAL REVIEW D **96,** 095025 (2017)

Inert two-Higgs-doublet model strongly coupled to a non-Abelian vector resonance

Felipe Rojas-Abatte,[*] Maria Luisa Mora,[†] Jose Urbina,[‡] and Alfonso R. Zerwekh[§]

Department of Physics and Centro Científico Tecnológico de Valparaíso, Universidad Técnica Federico Santa María, Valparaíso 1680, Chile

(Received 14 July 2017; published 21 November 2017)

We study the possibility of a dark matter candidate having its origin in an extended Higgs sector which, at least partially, is related to a new strongly interacting sector. More concretely, we consider an i2HDM (i.e., a Type-I two Higgs doublet model supplemented with a Z_2 under which the nonstandard scalar doublet is odd) based on the gauge group $SU(2)_1 \times SU(2)_2 \times U(1)_Y$. We assume that one of the scalar doublets and the standard fermion transform nontrivially under $SU(2)_1$ while the second doublet transforms under $SU(2)_2$. Our main hypothesis is that standard sector is weakly coupled while the gauge interactions associated to the second group is characterized by a large coupling constant. We explore the consequences of this construction for the phenomenology of the dark matter candidate and we show that the presence of the new vector resonance reduces the relic density saturation region, compared to the usual i2DHM, in the high dark matter mass range. In the collider side, we argue that the mono-Z production is the channel which offers the best chances to manifest the presence of the new vector field. We study the departures from the usual i2HDM predictions and show that the discovery of the heavy vector at the LHC is challenging even in the mono-Z channel since the typical cross sections are of the order of 10^{-2} fb.

DOI: 10.1103/PhysRevD.96.095025

I. INTRODUCTION

The discovery of the Higgs boson [1,2] crowned standard model (SM) with great success. However, the high energy physics community is unanimous to suspect that the SM is not a complete description of the nongravitational interactions. Three main open questions justify this general conviction: a natural origin for the electroweak scale, the origin of neutrino masses, and the origin of dark matter (DM). The first of these problems has motivated the construction of many extensions of the SM. Some of them are based on the elegant idea that the electroweak scale may be dynamically produced in the context of a new strong interaction. Of course, this proposal inevitably leads to the prediction a new composite sector. On the other hand, although many observations point out to the existence of DM, we have few clues about its nature. A very popular possibility is that DM consists of neutral massive particles (with masses ranging from some GeV's to some TeV's) with annihilation cross section of the same order of magnitude than the cross sections obtained from the weak interaction (the so-called WIMP). One of the best known models that incorporate this kind of DM candidate is a type-I 2HDM where one of the doublets is odd under a new (and usually *ad-hoc*) Z_2 symmetry. This model is usually referred as the inert two Higgs doublet model or i2HDM [3–5]. It is tempting to merge the ideas of an extended Higgs sector and compositeness, at least partially. Indeed already some authors have explored the phenomenology of the 2HDM in the context of traditional dynamical electroweak symmetry breaking [6] and the so-called composite Higgs models where the scalar doublets arise as pseudo-Nambu-Goldstone bosons [7–12]. Additionally, for some particular models, it has been studied the phenomenological consequences of a two Higgs doublet sector coupled to composite vector resonances [11,13]. In this paper, we focus on a i2HDM where one of the scalar doublets (the one which is odd under the Z_2 symmetry) is supposed to belong to a new strongly interacting sector and is directly coupled to a vector resonance. This is in consonance with the very appealing idea of having a complex hidden sector with its own interactions and structure levels. We explore mainly the consequences of the new heavy vector on the phenomenology of the DM candidate. Additionally we argue that the best chance to observe a signature of the new vector resonance at the LHC comes from the single production of a gauge boson plus missing transverse energy. To achieve our goals, we have organized our paper in the following way: in Sec. II we describe our theoretical construction emphasizing the introduction of the new heavy vector. In Sec. III we comment on the *a priori* experimental and theoretical constrains which are relevant for our model. In Sec. IV, we describe our results for the phenomenology of the DM candidate while in Sec. V we focus on the mono-Z production at the LHC. Finally in Sec. VI we state our conclusions.

[*] astrofis.rojas@gmail.com
[†] maria.luisa.mora.u@gmail.com
[‡] jose.urbina.avalos@gmail.com
[§] alfonso.zerwekh@usm.cl

II. THE MODEL

Following the idea of hidden local symmetry (HLS) [14], we introduce the new vector resonance as the effective gauge fields of a (hidden) gauge group which we call $SU(2)_2$. Consequently, our model is based on the local group $SU(2)_1 \times SU(2)_2 \times U(1)_Y$. We assume the first group is associated to the elementary or weak interacting sector while the second group describes a composite or strongly interacting sector. A fundamental hypothesis under our construction is that standard left-handed fermions and one of the scalar doublets (ϕ_1) transform under $SU(2)_1$ (and $U(1)_Y$) while the second scalar doublet (ϕ_2) transforms under $SU(2)_2$ (and the hypercharge group) as illustrated in Figure 1. Additionally, we introduce a bi-doublet field which transforms as $U_1 \Sigma U_2^\dagger$ with U_1 and U_2 elements of $SU(2)_1$ and $SU(2)_2$ respectively. With this ingredients, and assuming that ϕ_2 is odd under a new Z_2 symmetry, the most general Lagrangian (with operators up to dimension 4) for the gauge and scalar sector is

$$\begin{aligned}\mathcal{L} = &-\frac{1}{2}\mathrm{Tr}[F_{1\mu\nu}F_1^{\mu\nu}] - \frac{1}{2}\mathrm{Tr}[F_{2\mu\nu}F_2^{\mu\nu}] + \frac{u^2}{2}\mathrm{Tr}[(D_\mu\Sigma)^\dagger(D^\mu\Sigma)] \\ &+ (D_\mu\phi_1)^\dagger(D^\mu\phi_1) + (D_\mu\phi_2)^\dagger(D^\mu\phi_2) + m_1^2(\phi_1^\dagger\phi_1) \\ &+ m_2^2(\phi_2^\dagger\phi_2) - \lambda_1(\phi_1^\dagger\phi_1)^2 - \lambda_2(\phi_2^\dagger\phi_2)^2 - \lambda_3(\phi_1^\dagger\phi_1)(\phi_2^\dagger\phi_2) \\ &- \lambda_4(\phi_1^\dagger\Sigma\phi_2)(\phi_2^\dagger\Sigma^\dagger\phi_1) - \frac{\lambda_5}{2}[(\phi_1^\dagger\Sigma\phi_2)^2 + (\phi_2^\dagger\Sigma^\dagger\phi_1)^2]\end{aligned} \tag{1}$$

where

$$D_\mu\Sigma = \partial_\mu\Sigma - ig_1A_{1\mu}\Sigma + ig_2\Sigma A_{2\mu}$$
$$D_\mu\phi_j = \partial_\mu\phi_j - ig_jA_{j\mu}\phi_j - i\frac{g_y}{2}B_\mu$$

and u is an energy scale which characterize the new strong sector.

The $SU(2)_1 \times SU(2)_2$ is spontaneously broken down to the diagonal subgroup, which we identify with $SU(2)_L$, when the Σ field acquires a v.e.v $\langle\Sigma\rangle = 1$. In this phase, Lagrangian (1) becomes:

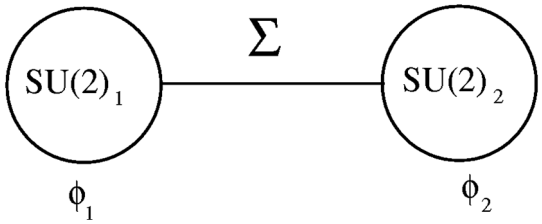

FIG. 1. Moose diagram representing the non-Abelian part of the group structure underlying our model. The Σ link field is a bi-doublet while the scalars ϕ_1 and ϕ_2 are doublets of $SU(2)_1$ and $SU(2)_2$ respectively.

$$\begin{aligned}\mathcal{L} = &-\frac{1}{2}\mathrm{Tr}[F_{1\mu\nu}F_1^{\mu\nu}] - \frac{1}{2}\mathrm{Tr}[F_{2\mu\nu}F_2^{\mu\nu}] \\ &+ \frac{u^2}{2}\mathrm{Tr}[(g_1A_{1\mu} - g_2A_{2\mu})(g_1A_1^\mu - g_2A_2^\mu)] \\ &+ (D_\mu\phi_1)^\dagger(D^\mu\phi_1) + (D_\mu\phi_2)^\dagger(D^\mu\phi_2) + m_1^2(\phi_1^\dagger\phi_1) \\ &+ m_2^2(\phi_2^\dagger\phi_2) - \lambda_1(\phi_1^\dagger\phi_1)^2 - \lambda_2(\phi_2^\dagger\phi_2)^2 - \lambda_3(\phi_1^\dagger\phi_1)(\phi_2^\dagger\phi_2) \\ &- \lambda_4(\phi_1^\dagger\phi)(\phi_2^\dagger\phi_1) - \frac{\lambda_5}{2}[(\phi_1^\dagger\phi_2)^2 + (\phi_2^\dagger\phi_1)^2]\end{aligned} \tag{2}$$

and a mass mixing term appears in the gauge sector. On the other hand, the electroweak symmetry breaking occurs, as in the SM, when ϕ_1 gets a vacuum expectation value (v.e.v): $\langle\phi_1\rangle = (0, v/\sqrt{2})^T$. Notice that we assume that ϕ_2 does not acquires a v.e.v. This fact assures that ϕ_1 is the SM Higgs doublet and forbid the appearance of any mass mixing term in the scalar sector. Finally, notice that, because of the same Z_2 symmetry, Yukawa terms can only be constructed with ϕ_1.

After these symmetry breaking processes, the following nondiagonal mass matrices are generated for the neutral and charged vector bosons:

$$M_N^2 = \frac{v^2}{4}\begin{bmatrix}(1+a^2)g_1^2 & -a^2g_1g_2 & -g_1g_y \\ -a^2g_1g_2 & a^2g_2^2 & 0 \\ -g_1g_y & 0 & g_Y^2\end{bmatrix}$$
$$M_C^2 = \frac{v^2}{4}\begin{bmatrix}(1+a^2)g_1^2 & -a^2gg_2 \\ -a^2g_1g_2 & a^2g_2^2\end{bmatrix}$$

where $a = u/v$ and g_1, g_2 and g_Y are the coupling constants associated to $SU(2)_1$, $SU(2)_2$, and $U(1)_Y$. When M_N^2 is diagonalized in the limit where $g_2 \gg g_1$, we obtain the following mass eigenstates for the neutral sector:

$$A_\mu = \frac{g_Y}{\sqrt{g_1^2+g_Y^2}}A_{1\mu}^3 + \frac{g_1g_Y}{g_2\sqrt{g_1^2+g_Y^2}}A_{2\mu}^3 + \frac{g_1}{\sqrt{g_1^2+g_Y^2}}B_\mu$$
$$Z_\mu = -\frac{g_1}{\sqrt{g_1^2+g_Y^2}}A_{1\mu}^3 - \frac{g_1^2}{g_2\sqrt{g_1^2+g_Y^2}}A_{2\mu}^3 + \frac{g_Y}{\sqrt{g_1^2+g_Y^2}}B_\mu$$
$$\rho_\mu^0 = -\frac{g_1}{g_2}A_{1\mu}^3 + A_{2\mu}^3.$$

where ρ denotes the new heavy vector resonance.

Similarly, the eigenstates of the charged sector (in the same limit) are:

$$W_\mu^\pm = A_{1\mu}^\pm + \frac{g_1}{g_2}A_{2\mu}^\pm$$
$$\rho_\mu^\pm = -\frac{g_1}{g_2}A_{1\mu}^\pm + A_{2\mu}^\pm$$

where, as usual, $A_{n\mu}^\pm = \frac{1}{\sqrt{2}}(A_{n\mu}^1 \mp A_{n\mu}^2)$.

In the same limit, the masses of the vector states can me expressed as:

$$M_A = 0 \qquad \text{(exact)} \tag{3}$$

$$M_Z \approx \frac{v\sqrt{g_1^2+g_y^2}}{2}\left[1-\frac{1}{2}\frac{g_1^4}{g_2^2(g_1^2+g_y^2)}\right] \tag{4}$$

$$M_{\rho^0} \approx \frac{avg_2}{2}\left[1+\frac{g_1^2}{2g_2^2}\right] \tag{5}$$

$$M_W \approx \frac{vg_1}{2}\left[1-\frac{g_1^2}{2g_2^2}\right] \tag{6}$$

$$M_{\rho^\pm} \approx \frac{avg_2}{2}\left[1+\frac{g_1^2}{2g_2^2}\right]. \tag{7}$$

Notice that to first order in g_1/g_2, we can write:

$$\frac{g_1}{g_2} \approx a\frac{M_W}{M_\rho}.$$

The quantity g_1/g_2 is supposed to be small. This is the precise meaning of the assumption that the nonstandard sector is strongly interacting. As we will explain below, in this work we consider values of M_ρ in the 2–4 TeV range and $a = 3, 4, 5$, obtaining $g_1/g_2 < 0.2$.

In the scalar sector, the spectrum is straightforward since, as we already emphasized, no mass mixing term arise due to the Z_2 symmetry. Consequently, near the minimum of the potential, the scalar doublets can be parametrized as:

$$\phi_1 = \frac{1}{\sqrt{2}}\begin{pmatrix} 0 \\ v+H \end{pmatrix} \quad \phi_2 = \frac{1}{\sqrt{2}}\begin{pmatrix} \sqrt{2}h^+ \\ h_1+ih_2 \end{pmatrix} \tag{8}$$

where H is the SM-like Higgs boson and is identified with the observed 125 GeV scalar state. Notice that the Z_2 symmetry makes the lightest component of ϕ_2 stable. As it is usually done, we assume that h_1 is the stable state and, consequently, the DM candidate.

Our model has seven free parameters: u, g_2, m_2, and λ_i with $i = 2\ldots5$ (λ_1 is fixed by the mass of the 125 GeV scalar observed at the LHC), however not all of them are equally significant for our research. It is convenient, for phenomenological proposes to work with the following parameters:

$$M_{h_1}, \quad M_{h_2}, \quad M_{h^\pm}, \quad M_\rho, \quad \lambda_{345}, \quad \lambda_2, \quad a \tag{9}$$

where $M_{h_1}, M_{h_2}, M_{h^\pm}$ are the physical masses of the new scalars, M_ρ is the mass of the vector resonance and $\lambda_{345} = \lambda_3 + \lambda_4 + \lambda_5$. Notice that λ_{345} plays a crucial roll controlling the interaction between the dark matter and the SM Higgs. According to this, we can rewrite the coupling constants as a function of the free parameters

$$\lambda_3 = \lambda_{345} + 2\frac{M_{h^\pm}^2 - M_{h_1}^2}{v^2} \qquad \lambda_4 = \frac{M_{h_1}^2 + M_{h_2}^2 - 2M_{h^\pm}^2}{v^2}$$
$$\lambda_5 = -\frac{M_{h_2}^2 - M_{h_1}^2}{v^2} \quad m_2^2 = \lambda_{345}\frac{v^2}{2} - M_{h_1}^2 \quad g_2 = \frac{2M_\rho}{va}. \tag{10}$$

III. EXPERIMENTAL AND THEORETICAL CONSTRAINS

The model parameter space can be constrained from theoretical restrictions coming from the analysis of the potential and experimental searches as well. In this section we mention all the restriction that we are account.

(i) *Vacuum stability:* In order to perform calculations around a minimum point without loose stability of the potential we need that there is no direction in field space along which the potential tends to minus infinity. This leads to the well-known conditions [15]

$$\lambda_1 > 0, \qquad \lambda_2 > 0, \qquad 2\sqrt{\lambda_1\lambda_2} + \lambda_3 > 0,$$
$$2\sqrt{\lambda_1\lambda_2} + \lambda_3 + \lambda_4 + \lambda_5 > 0 \tag{11}$$

It is worth it to note that the authors of Ref. [16] show that considering loop corrections to the vacuum stability some regions of the parameter space which originally were forbidden are reopen and, although this offer an opportunity to revisit the phenomenology the i2HDM, in this work we follow a more conservative approach and we consider the generally accepted stability conditions quoted above.

(ii) *Neutral vacuum:* Another important requirement is that the vacuum must be electrically neutral. This can be guarantied if

$$\lambda_5 < 0 \quad \text{and} \quad \lambda_4 + \lambda_5 < 0 \tag{12}$$

The last condition [Eq. (12)] assures us that M_{h_1} is the lightest particle which is odd under the Z_2 symmetry.

(iii) *Inert vacuum:* We need to consider the case where only the standard model field ϕ_1 get a vacuum expectation value in order to avoid a mixing term between dark matter and the Higgs boson which will be catastrophic for abundance of relic density. According to Ref. [17] the vacuum stability condition is satisfied provided that:

$$m_1^2 > 0 \quad \text{and} \quad m_2^2 < \sqrt{\frac{\lambda_2}{\lambda_1}} m_1^2. \tag{13}$$

In terms of our set of independent parameters, these conditions translate into:

$$M_{h_1}^2 > \frac{v^2}{2}\left(\lambda_{345} - 2\sqrt{\lambda_1\lambda_2}\right). \tag{14}$$

This is a very important constraint because it places an upper bound on λ_{345} for a given DM mass M_{h_1}.

(iv) *Perturbatibity:* All the quartic couplings of the potential must be limited by perturbativity constraint, therefore

$$|\lambda_i| \leq 8\pi \tag{15}$$

(v) *Unitarity:* According to Ref. [18] we can impose tree-level unitarity constraints if the eigenvectors of the scattering matrix elements between scalars and gauge bosons satisfy

$$|e_i| \leq 8\pi \tag{16}$$

where the parameters e_i are defined as

$$e_{1,2} = \lambda_3 \pm \lambda_4, \qquad e_{3,4} = \lambda_3 \pm \lambda_5 \tag{17}$$

$$e_{5,6} = \lambda_3 + 2\lambda_4 \pm 3\lambda_5,$$
$$e_{7,8} = -\lambda_1 - \lambda_2 \pm \sqrt{(\lambda_1 - \lambda_2)^2 + \lambda_4^2} \tag{18}$$

$$e_{9,10} = -3\lambda_1 - 3\lambda_2 \pm \sqrt{9(\lambda_1 - \lambda_2)^2 + (2\lambda_3 + \lambda_4)^2} \tag{19}$$

$$e_{11,12} = -\lambda_1 - \lambda_2 \pm \sqrt{(\lambda_1 - \lambda_2)^2 + \lambda_5^2} \tag{20}$$

On the other hand, the introduction of a massive vector resonance may, in principle, induce dangerous perturbative unitarity violating processes. However, in our construction, the potentially problematic $W^+W^-\rho^0$ vertex is highly suppressed being of the order of $g_1\cos(\theta_W)\left(\frac{g_1^3}{g_2^3}\right)\left(\frac{v^2}{u^2}\right)$, where θ_W is Weinberg's angle. Although this is well beyond the level of approximation we are working at, we estimated the contribution to perturbative unitarity violation in the channel $W_LW_L \to W_LW_L$. We found that the corresponding scale of unitarity violation is

$$\Lambda_{\text{uv}} \approx \left(\frac{2\sqrt{6\pi}M_\rho M_Z}{M_W u}\right)^{1/2} \frac{M_\rho}{M_W} v.$$

In our case, the lowest value of Λ_{uv} is obtained for $u = 5v \approx 1.2$ TeV and $M_\rho = 2$ TeV, thus we found that $\Lambda_{\text{uv}} > 25$ TeV. This has to be compared with the maximum scale at which our model remains valid: $4\pi u \sim 9$–15 TeV.

(vi) *Electroweak precision test:* In the i2HDM the electroweak radiative corrections are affected by the relation between the scalar masses [5] alongside the Higgs mass and Z boson mass. The expressions for the S and T values are

$$S = \frac{1}{72\pi}\frac{1}{(x_2^2 - x_1^2)^3}\left[x_2^6 f_a(x_2) - x_1^6 f_a(x_1) + 9x_2^2x_1^2(x_2^2 f_b(x_2) - x_1^2 f_b(x_1))\right] \tag{21}$$

where $x_1 = \frac{M_{h_1}}{M_{h^\pm}}$, $x_2 = \frac{M_{h_2}}{M_{h^\pm}}$, $f_a(x) = -5 + 12\log(x)$, $f_b(x) = 3$–$4\log(x)$ and

$$T = \frac{1}{32\pi^2\alpha v^2}\left[F(M_{h^\pm}^2, M_{h_2}^2) + F(M_{h^\pm}^2, M_{h_1}^2) - F(M_{h_2}^2, M_{h_1}^2)\right] \tag{22}$$

where the function $F(x, y)$ is defined by

$$F(x,y) = \begin{cases} \frac{x+y}{2} - \frac{xy}{x-y}\log\left(\frac{x}{y}\right), & x \neq y \\ 0, & x = y. \end{cases}$$

Written in this form, according to Ref. [19], the contribution to S and T shows explicitly that we cannot distinguish the CP properties of h_1 and h_2. With U fixed to be zero, the central value of S and T, assuming a SM Higgs boson mass of $m_h = 125$ GeV, are given by [20]

$$S = 0.06 \pm 0.09, \quad T = 0.1 \pm 0.07 \tag{23}$$

with the correlation coefficient $+0.91$.

Concerning the consistency of the introduction of the new vector resonance with the electroweak precision tests, we computed the tree level correction to the T parameter due to the presence of the new vector boson. Our result is

$$\Delta T_{\text{tree}} \approx \frac{\tan^2(\theta_W) {M_W}^6 a^2}{\alpha_{\text{EM}} {M_\rho}^6}.$$

For the values of a and M_ρ considered in this work, ΔT_{tree} turns out to be very small: $\Delta T_{\text{tree}} \sim 10^{-9}$–$10^{-5}$ which is in perfect agreement with current limits on ΔT at 95% C.L. Additionally, in models with very massive vector resonances it is expected that the S parameter be proportional to T [21] and, consequently, we expect ΔS_{tree} to be

also small. In what respect to loop contributions, our experience which models containing heavy vector resonances [22,23] shows that for small mixing angle and large resonance mass (as is our case), the one-loop contribution are consistent with experimental limits.

(vii) *LHC constrains on vector resonances:* In general, vector resonances may produce detectable signals at colliders through channels like dijet production, dilepton production, the associate production of a Higgs boson and a gauge boson, and the production of two gauge bosons. Also the Higgs decay rate into two photons (which is loop process) and the oblique parameter S, T may receive sensible corrections from heavy charged fields. However, in our case the new vector resonance couples to the SM fields only through mixing terms which are suppressed by factors g_1/g_2. Moreover, previous studies suggest that the experimental constrains are largely satisfied if the new resonance is heavier than 2.4 TeV [22,24,25]. As a matter of example, we compare the cross section predicted by our model for the process $pp \to \rho_\mu \to jj$ with the upper limits set by ATLAS for dijet resonances [26], as shown in Fig. 2. Our calculations are performed in two different kinematic regimes depending on whether the ρ_μ decay channels into a pair of nonstandard scalars are open or not. When these channels are open they dominate over the decay into SM particles since the interaction in the former case is proportional to g_2 while in the latter case is suppressed by a factor g_1/g_2. This makes the resonant dijet production quit unprovable as shown by the lowest continuous line in Figure 2. The upper continuous line, on the other hand, shows the predicted cross section when the vector resonance is not able to decay into nonstandard scalars. Notice that in the appropriate kinematic regime, values of $M_\rho < 2.4$ TeV are allowed.

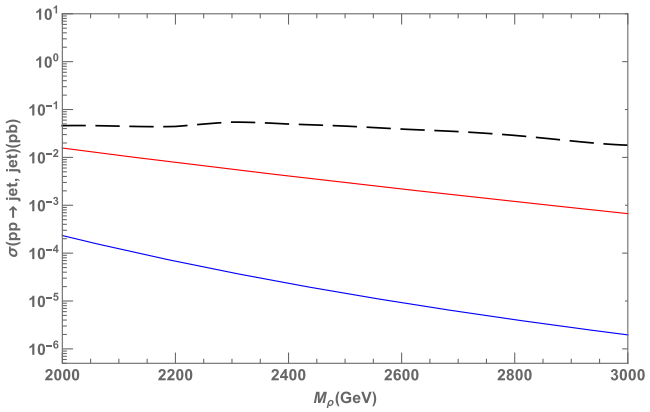

FIG. 2. $\sigma(pp \to \rho_\mu \to jj)$ computed in the kinematic region where the ρ_μ decay channels into a pair of nonstandard scalars are open (lower solid line) or closed (higher solid line). In both cases we used $a = 3$. The predictions are compared to the upper limits set by ATLAS for dijet resonances (dashed line).

(viii) *LHC limits from Higgs di-photon decay:* The decay rate of the Higgs bosons into two photons does not constrain very much the mass of the vector resonance either because the Higgs boson couples to ρ_μ only as a result of the mixing between $A_{1\mu}$ and $A_{2\mu}$ and, consequently, the $H\rho_\mu^+\rho_\nu^-$ vertex is suppressed by a factor $(g_1/g_2)^2$. However, the interaction vertex $Hh_\mu^+h_\nu^-$ is governed by the λ_3 quartic coupling which can be constrained through loop calculations. We can use the limit coming from ATLAS-CMS Higgs data analysis [27] to set a restriction on λ_3 using the experimental value:

$$\frac{\mathrm{Br}^{BSM}(H \to \gamma\gamma)}{\mathrm{Br}^{\mathrm{SM}}(H \to \gamma\gamma)} = \mu^{\gamma\gamma} = 1.16^{+40}_{-36} \qquad (24)$$

(ix) *Invisible Higgs-decay:* Interactions among Higgs boson and the new sector (inert scalars and vector resonance) are allowed in this model, therefore the possibility of new invisible decay channels are open. Those channels could lead to deviations of Higgs boson decay width from the SM value. Using results that comes from ATLAS [28] at 95% CL we can restrict the invisible Higgs decay to be less than

$$\mathrm{Br}(H \to \text{invisible}) < 28\% \qquad (25)$$

which is also compatible with the CMS result [29].

(x) *LEP limits on inert scalars:* In order to not affect the precise measurements of W and Z widths we need to impose restrictions to the mass of the inert scalars demanding that $\Gamma(W^\pm \to h_1 h^\pm)$, $\Gamma(W^\pm \to h_2 h^\pm)$, $\Gamma(Z \to h_1 h_2)$ and $\Gamma(Z \to h^+ h^-)$ channels are kinematically closed. This leads to the following constraints:

$$\begin{aligned} &M_{h_1} + M_{h^\pm} > M_{W^\pm} \qquad M_{h_2} + M_{h^\pm} > M_{W^\pm} \\ &M_{h_1} + M_{h_2} > M_Z \qquad 2M_{h^\pm} > M_Z \end{aligned} \qquad (26)$$

(xi) *Relic density limits:* We analyze the abundance of dark matter using MICROMEGAS [30–32] package. This program solves the Boltzmann equation numerically, using CALCHEP [33] to calculate all of the relevant cross sections. The program consider the case when $M_{h_1} < M_W, M_Z$ taking into account the annihilation into 3-body final state from VV^* or 4-body final state from V^*V^* ($V = W^\pm, Z$). Coannihilation effects are taken into account as well. We require that our predictions for the relic

density be in agreement with the PLANCK [34,35] measurement:

$$\Omega_{\rm DM}^{\rm Planck}h^2 = 0.1184 \pm 0.0012. \quad (27)$$

(xii) *Direct detection limits:* Using the first dark matter results coming from XENON1T [36] with 34.2 live days of data acquired between November 2016 and January 2017 we have evaluated the spin-independent cross section of DM scattering off the proton, σ_{SI}, also using MICROMEGAs.

IV. DARK MATTER PHENOMENOLOGY

As we explained above, our model has a 7-dimensional parameter space, however we can have a good phenomenological overview of the model focusing only on 3 specific parameters (λ_{345}, M_{h_1}, M_ρ) and fixing all the other ones to which the phenomenological observables have poor sensibility. For instance, the dark matter candidates and the SM fields only interact through the Higgs boson, the electroweak gauge bosons and the new heavy vector; but, since the interaction with the standard gauge bosons is governed by the electroweak gauge couplings which are fixed, the only relevant free parameter is λ_{345}, the dark matter mass itself (M_{h_1}) and M_ρ.

In Fig. 3 we show a 2-dimensional section of the parameter space where we have the dark matter relic density as a function of M_{h_1} for several values of λ_{345}. For simplicity, in this analysis we always take $M_{h_2} = M_{h^\pm}$. With this assumption an important kinematic parameter is $\Delta M \equiv M_{h_2} - M_{h_1}$. Now, two qualitatively different scenarios can be distinguished: a quasidegenerate case where $\Delta M = 1$ GeV and a nondegenerate case $\Delta M = 100$ GeV. In both we considere $M_\rho = 3000$ GeV, $a = 2$ and $\lambda_2 = 1$. We can notice that for 10 GeV $\leq M_{h_1} \ll M_\rho/2$ GeV (which we will refer as the low mass region) the model reproduces the same pattern of relic density predicted by the usual the i2HDM, as expected. It is only when M_{h_1} approaches to $M_\rho/2$ that the effect of the vector resonance ρ becomes important.

In Ref. [19] there is a detailed phenomenological explanation of what happens in the low mass region, so we will just briefly comment on it. Here, we can distinguish two different asymptotic behaviors: the first one for 10 GeV $< M_{h_1} <$ 50 GeV and the second one ($M_{h_1} > 200$) GeV.

In Fig. 3(a), which shows the quasidegenerate case, we can see that below 62.5 GeV (i.e., half of the Higgs boson mass) the coannihilation effects between the inert scalars become important because of the appearance of new annihilation channels, pushing the DM relic density under the experimental PLANCK limit. On the other hand, in the non-degenerate case (when $\Delta M = 100$ GeV), as seen in Fig. 3(b), coannihilation is suppressed generating an enhancement of the $\Omega_{\rm DM}h^2$ becoming even 3 orders of magnitude above the PLANCK limit for small values of λ_{345} ($\sim$0.01).

Now, in the second case (i.e., for $M_{h_1} > 200$ GeV), when $\Delta M = 1$ GeV the quartic coupling becomes small enough to produce a significant suppression of the dark matter annihilation into longitudinal polarized gauge bosons. This effect increases the relic density which is capable of reaching the PLANCK limit even considering the effects of co-annihilation. On the other hand, for the nondegenerate case, as seen in Fig. 3(b), the value ΔM is

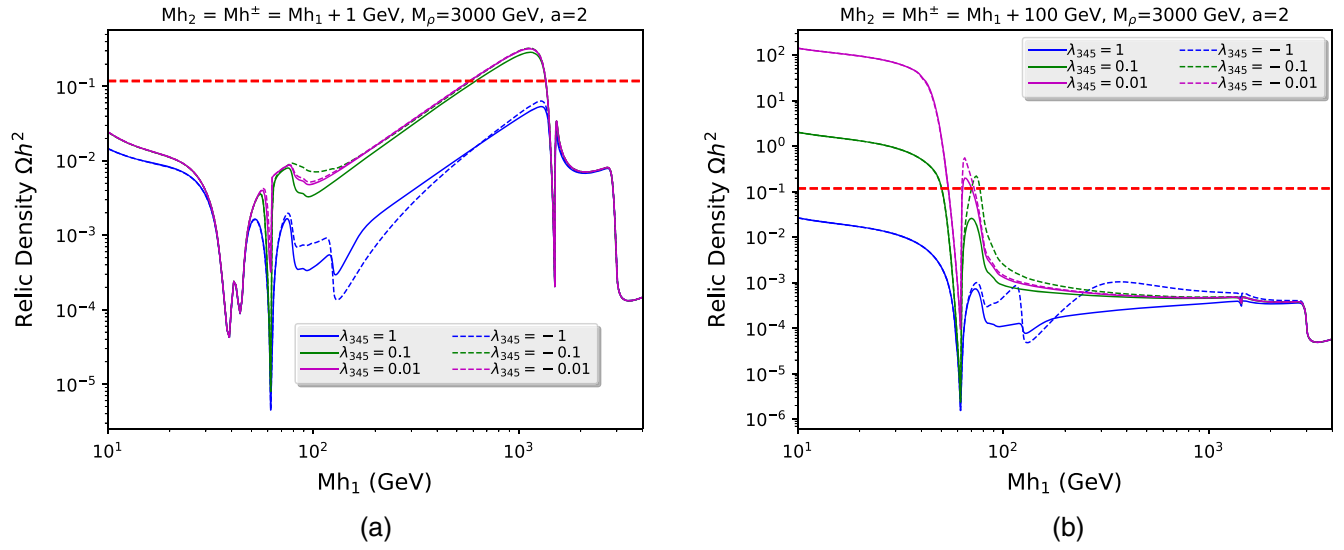

FIG. 3. Relic density $\Omega_{\rm DM}h^2$, as a function of M_{h_1} for different values of λ_{345} in a quasidegenerate scenario (a) where $M_{h_2} = M_{h^\pm} = M_{h_1} + 1$ and a no-degenerate scenario (b) where $M_{h_2} = M_{h^\pm} = M_{h_1} + 100$. In both cases we fix the values of $M_\rho = 3000$ GeV, $a = 2$ and $\lambda_2 = 1$. The horizontal red line corresponds to the relic density measurements PLANCK limits.

TABLE I. Range of the parameter space.

Parameter	Min value	Max value
M_{h_1} [GeV]	480	4500
M_{h_2} [GeV]	480	4500
$M_{h^\pm}$ [GeV]	480	4500
M_ρ [GeV]	2500	4500
λ_{345}	−5	5
λ_2	0	5
a	3	5

large and the average annihilation cross sections of the processes $h_1h_1 \to W_LW_L$ and $h_1h_1 \to Z_LZ_L$ are increased, making the abundance of relic density too low to reach the saturation limit. This generates the flat asymptotic behavior for large values of M_{h_1}.

When $\Omega_{\rm DM}h^2$ reaches the PLANCK limit in the high mass region, but now considering the $\Delta M = 1$ GeV case, the annihilation average cross section through the vector resonance starts to be important as the value of M_{h_1} increases. At $M_{h_1} = M_\rho/2$ GeV the value of the relic density distribution decreases dramatically due to co-annihilation of h_1 and h_2 into an on-shell ρ vector. The wide deep around 3000 GeV [see Fig. 3a)] corresponds to the opening of annihilation channels $h^+h^- \to \rho \to \rho^+\rho^-$, $h_1h_1 \to \rho^+\rho^-$, and $h_2h_2 \to \rho^+\rho^-$. In the case where $\Delta M = 100$ GeV, the main annihilation processes are $h_1h_1 \to W^+W^-$ and $h_1h_1 \to ZZ$, although there is a small contribution (∼4%) of the process $h_1h^+ \to \rho^+H$ via s-channel ρ boson interchange which generate the small negative peak at $M_{h_1} = M_\rho/2$. Finally, in this case, the last deep at $M_{h_1} = 3000$ GeV is produced through the opening of the annihilation channels $h_1h_1 \to \rho^+\rho^-$ and $h_1h_1 \to \rho^0\rho^0$.

In order to have a complete visualization of how the vector resonance affects the i2HDM, we performed a random scan over the 7-dimensional parameter space considering all the experimental and theoretical constraints mentioned in Sec. III. In our analysis, we exclude all the points in the parameter space where overabundance take place because they are considered nonphysical. However, we keep the regions of points which produce underabundance since it only means that an additional source of DM is needed. Consequently, we used a rescaled direct detection cross section $\hat{\sigma}_{\rm SI} = (\Omega_{\rm DM}/\Omega_{\rm PLANCK}) \times \sigma_{\rm SI}$ which allows us to take into account the case when h_1 contribute only partially to the total amount of DM. The range of the scan for each free parameter is summarized in Table I.

As it was previously explained, our model reproduces the same pattern of $\Omega_{\rm DM}h^2$ as the i2HDM for $M_{h_1} \ll M_\rho/2$ because the interaction between the SM particles and the vector resonance (ρ_μ) is suppressed by the factor (g_1/g_2). Therefore we will focus on the high mass region where the interaction with the vector resonance is more sensitive.

In Figure 4, we show projections in 2-dimensional planes of the scan as a color map of DM relic density where we show the planes (M_{h_1}, λ_{345}) and (M_{h_1}, M_ρ). In Fig. 4(a), we can see the effect of the vacuum stability constraint on λ_{345}, making it to satisfy the bound $\lambda_{345} \gtrsim -1.47$.

It is easy to recognize the DM annihilation into an on-shell vector resonance $(h_1h_2 \to \rho)$ at $M_{h_1} \approx M_\rho/2$ GeV through the substantial DM relic density decrease in a narrow sector represented by the diagonal blue pattern in Fig. 4(b).

It is important to stress that $M_\rho/2$ establishes a border in the parameter space for the saturation of relic density. For $M_{h_1} > M_\rho$, the annihilation cross section becomes more intense and the abundance of relic density decreases below the experimental PLANCK limit. This border is clearly seen in Fig. 5(b) where we present the parameter space which at the same time reproduces the value of $\Omega_{\rm DM}h^2$ observed by PLANCK and is consistent with all the

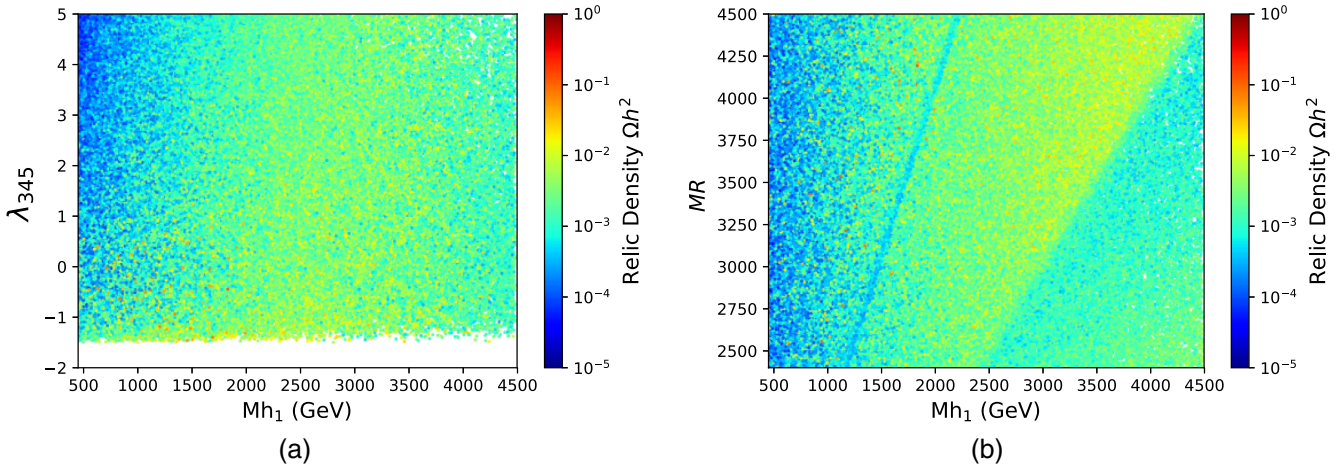

FIG. 4. 2D projections of the 7D random scan of the model parameter space restricted to (450 GeV, 4500 GeV) for M_{h_1}, (2500 GeV, 4500 GeV) for M_ρ and $(-2, 5)$ for λ_{345} considering all constraints except under-abundance of DM.

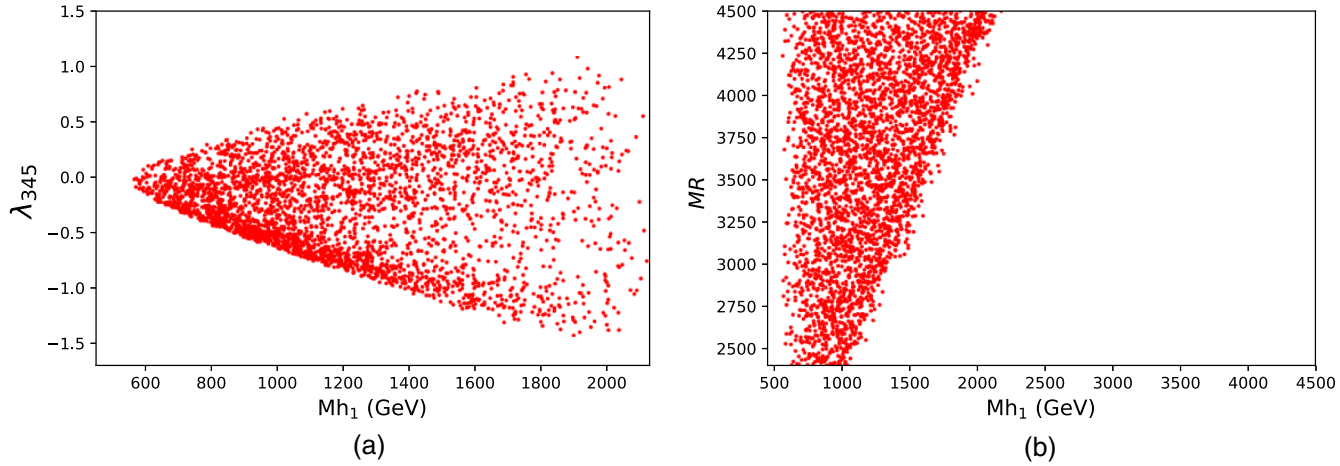

FIG. 5. 2D projections of the 7D random scan of the model parameter space restricted to (450 GeV, 4500 GeV) for M_{h_1}, (2500 GeV, 4500 GeV) for M_ρ and $(-2, 5)$ for λ_{345} considering all constraints plus the lower PLANCK limit.

experimental constrains. In other words, the interactions due to the new vector resonance reduce the saturation region in the high mass zone compared to i2HDM because when the DM reaches the limit $M_{h_1} \approx M_\rho$ the channels $h_1 h_2 \to \rho^+ \rho^-$ and $h_1 h_2 \to \rho^0 \rho^0$ become open causing the abundance of DM to fall down by at least one order of magnitude, as we can clearly see from Fig. 4(b).

As we stressed before, in the high mass zone it is possible to reach the saturation limit of the relic density due to the high level of degeneracy of the three inert scalars, which turns out to be no more than a few GeV. This mass split is closely related to the quartic coupling of the potential. A small difference of mass implies small values of the λ parameters which translates into a low average annihilation cross section of the dark matter into longitudinal polarized gauge bosons, generating an enhancement in the abundance of relic density. This can be seen in Figs. 3(a) and 5(a) where λ_{345} can reach higher values as M_{h_1} increases. This effect is maintained until the threshold is reached at $M_{h_1} = 2250 = M_\rho^{\mathrm{MAX}}/2$ GeV, where $M_\rho^{\mathrm{MAX}} = 4500$ GeV is the maximum value of M_ρ used in our parameter space.

V. PREDICTIONS FOR THE LHC: MONO-Z PRODUCTION

At the LHC, the new vector resonance is mainly produced by quark annihilation. In consequence, the total production cross section $\sigma(pp \to \rho)$ is proportional to $(g_1/g_2)^2 \approx a^2 M_W^2/M_\rho^2$. In Fig. 6 we show our predictions for $\sigma(pp \to \rho^0)$ at the LHC with $\sqrt{s} = 13$ TeV. The tiny cross sections indicate that it is a very challenging task to discover the new heavy vector at the LHC specially when we consider only standard particles in the final states, since the interaction of the heavy vector with particles of the SM is suppressed by factors (g_1/g_2).

However, we can expect to have a better chance of getting observable signals if we consider final states containing the new scalar alongside some standard particle. A promising process is $pp \to h_1 h_1 V$ (with $V = Z$ or $W^\pm$). In this process the scalars are not detected but they produce a significant amount of missing transverse energy, as shown in Fig. 7 (right). Hereafter, we focus on the mono-Z production. Figure 7 (left) shows the predicted cross section for the process $pp \to \rho \to h_1 h_1 Z$ computed for three values of the a parameter ($a = 3$, 4, 5) while other relevant parameters were took as $M_{h1} = 800$ GeV, $M_{h2} = M_{h^\pm} = 810$ GeV, $\lambda_{345} = -0.1$ and $\lambda_2 = 2.0$. As

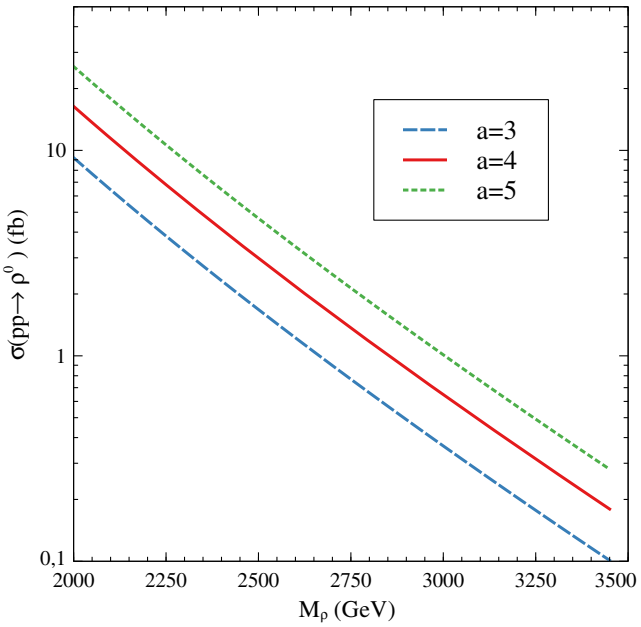

FIG. 6. $\sigma(pp \to \rho^0)$ vs $M\rho$ at the LHC for $\sqrt{s} = 13$ TeV.

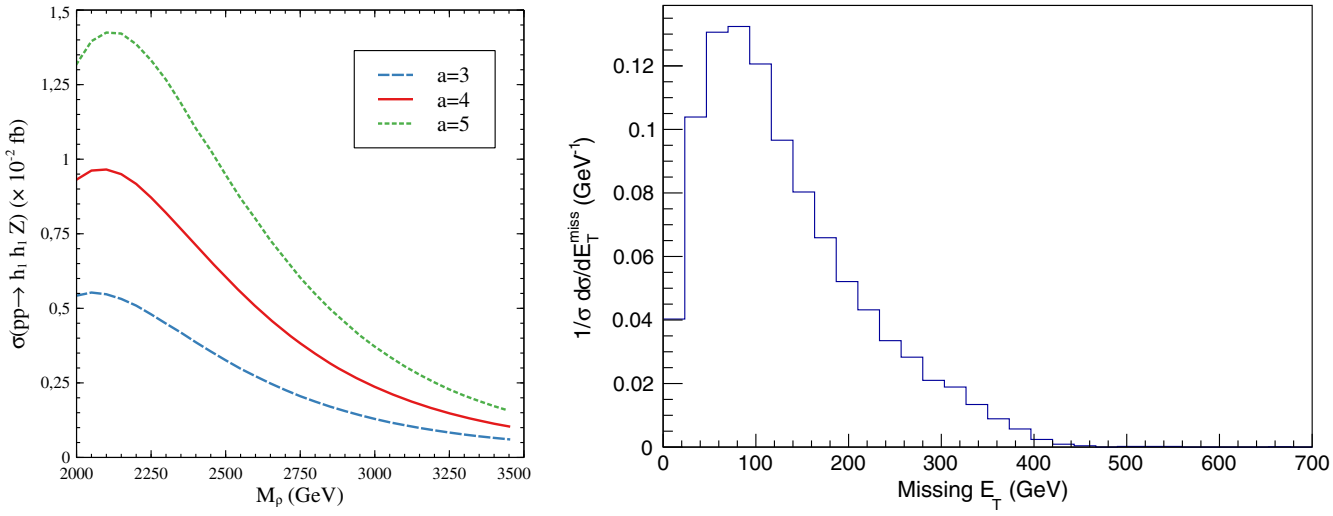

FIG. 7. Left: $\sigma(pp \to h_1 h_1 Z)$ at the LHC for $\sqrt{s} = 13$ TeV, $a = 3$ (dashed), $a = 4$ (continuous), $a = 5$ (dotted). We use $M_{h1} = 800$ GeV, $M_{h2} = 810$ GeV, $\lambda_{345} = -0.1$ and $\lambda_2 = 2.0$. Right: Normalized missing E_T distribution.

we see, for M_ρ between 2 and 3.5 TeV, the cross section lies in the range of $(0.05\text{–}1.5) \times 10^{-2}$ fb.

In order to compare the predictions of our model to the usual i2DHM ones, we compute $\sigma(pp \to h_1 h_1 Z)$ for the benchmark points 1 and 6 of Ref. [19] defined by $M_{h1} = 55$ GeV, $M_{h2} = 63$ GeV, $M_{h^\pm} = 150$ GeV, $\lambda_{345} = 1.0 \times 10^{-4}$, $\lambda_2 = 1.0$ (BM1) and $M_{h1} = 100$ GeV, $M_{h2} = 105$ GeV, $M_{h^\pm} = 200$ GeV, $\lambda_{345} = 2.0 \times 10^{-3}$, $\lambda_2 = 1.0$ (BM6) respectively. The computed cross sections include the kinematic cut $\not{E}_T > 100$ GeV for both benchmark points. In Figure 8, we show our results, alongside the cross section predicted in the usual i2HDM, for BM1 (left) and BM6 (right). In both cases we can see an important enhancement in the low M_ρ region compared to the usual i2DHM.

Additionally, we show in Fig. 9 our prediction for $\sigma(pp \to h_1 h_2 Z)$ at the $\sqrt{s} = 13$ TeV LHC considering the benchmark point BM6. This process also contributes to the mono-Z production provided that the mass splitting between h_1 and h_2 is small.

Finally, we analyze the observability of our signal using the package CHECKMATE [37]. We use experimental results obtained at the LHC for $\sqrt{s} = 8$ and a luminosity of 20.3 fb^{-1}. Then we extrapolate our results for a higher

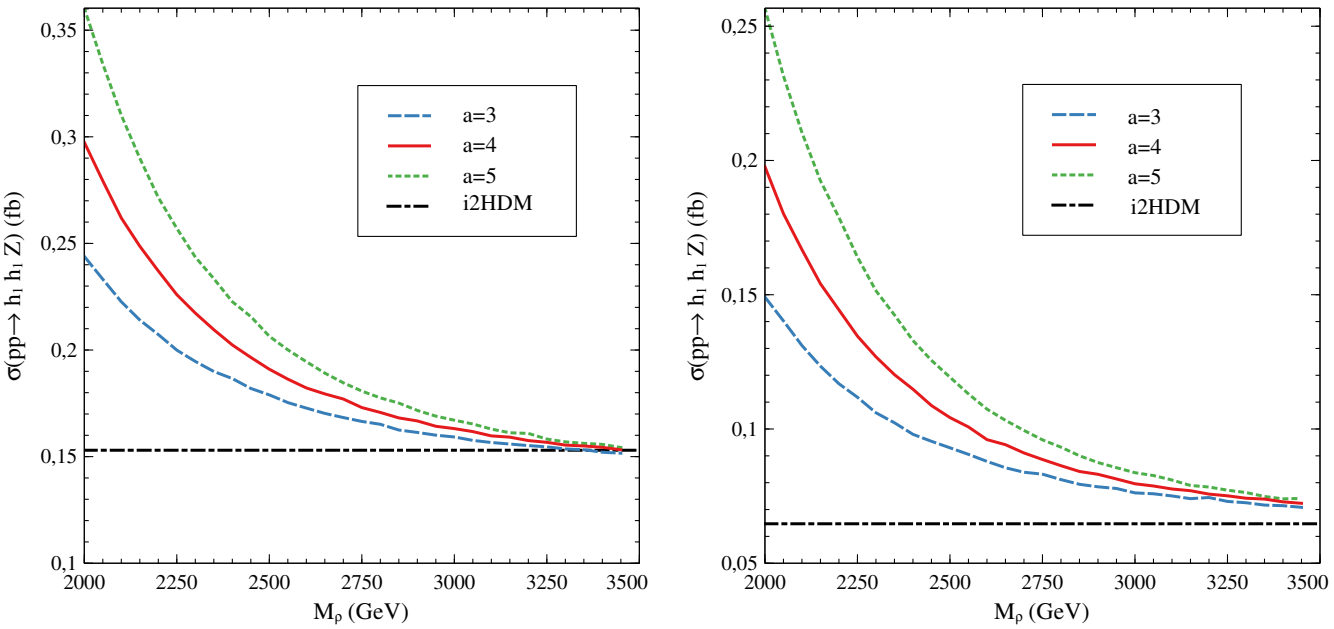

FIG. 8. Left: $\sigma(pp \to h_1 h_1 Z)$ vs M_ρ at the $\sqrt{s} = 13$ TeV LHC considering the benchmark point BM1. Right: *Idem* but for the benchmark point BM6.

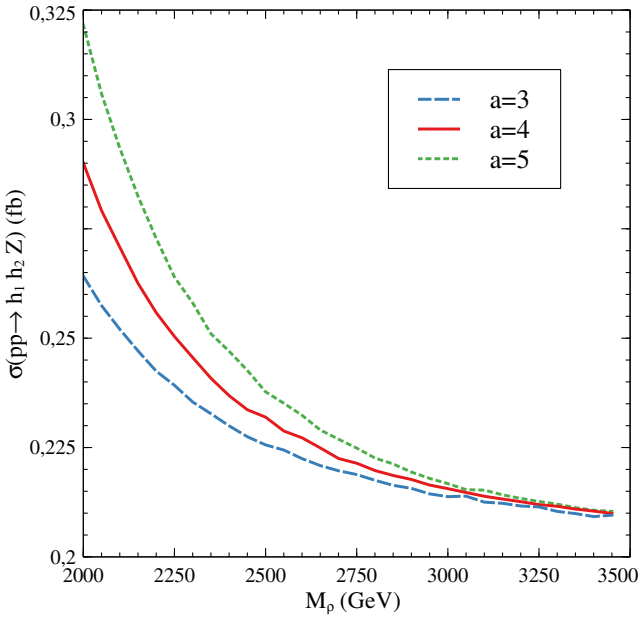

FIG. 9. $\sigma(pp \to h_1 h_2 Z)$ vs M_ρ at the $\sqrt{s} = 13$ TeV LHC considering the benchmark point BM6.

luminosity ($L = 3000$ fb^{-1}) at $\sqrt{s} = 13$ TeV using the formula:

$$\sigma_{13} = \sigma_8 \sqrt{\frac{\mathcal{L}}{\mathcal{L}'}} \sqrt{\frac{\sigma_b^{13}}{\sigma_b^8}} \tag{28}$$

where σ_8 (σ_{13}) is the minimum observable cross section for the LHC at $\sqrt{s} = 8$ TeV ($\sqrt{s} = 13$ TeV), σ_b^8 (σ_b^{13}) is the background cross section associated to the signal, $\mathcal{L} = 20.3$ fb^{-1} and $\mathcal{L}' = 3000$ fb^{-1}. The results are shown in Fig. 10. Unfortunately, even in the high luminosity regime the signal for mono-Z is two order of magnitude below the minimum observable cross section for generalistic kinematical cuts and only a dedicated search with a more specific approach can improve this situation.

VI. CONCLUSIONS

In this work, we have extended the i2DHM by adding a new heavy vector triplet and assuming that the inert scalar doublet is strongly coupled to the new spin-1 field. The theoretical construction was based on the hidden local symmetry idea and thus the new vector field was introduced by enlarging the gauge symmetry to $SU(2)_1 \times SU(2)_2 \times U(1)_Y$. The hypothesis of a strong interaction between the heavy vector field and the inert scalar doublet was implemented making the inert scalar field to be a doublet of $SU(2)_2$ while the standard field (including the Higgs filed) were supposed to transform nontrivially only under $SU(2)_1$.

In general, the model is allowed by current data provided that $M_\rho > 2.4$ TeV but lower values of M_ρ are possible when the decay of the new vector into nonstandard scalar is open. Indeed, in this kinematic region the discovery of ρ seems to be rather challenging at the LHC specially when it is considered its decay only into standard particles. A more interesting possibility is the production of a Z boson in association with two h_1 particles since the total process (ρ production and decay) is less suppressed than the previous case. Naturally, the h_1 particles would escape detection but they will produce a significant amount of missing transverse momentum. However, the predicted cross sections are quite small, although an important enhancement with respect to the usual i2DHM is observed for lower values of M_ρ, lying in the [0.1–0.3] fb range. Unfortunately, even considering this enhancement and a luminosity as high as 3000 fb^{-1}, the observation of this channel seems to be very challenging at the LHC.

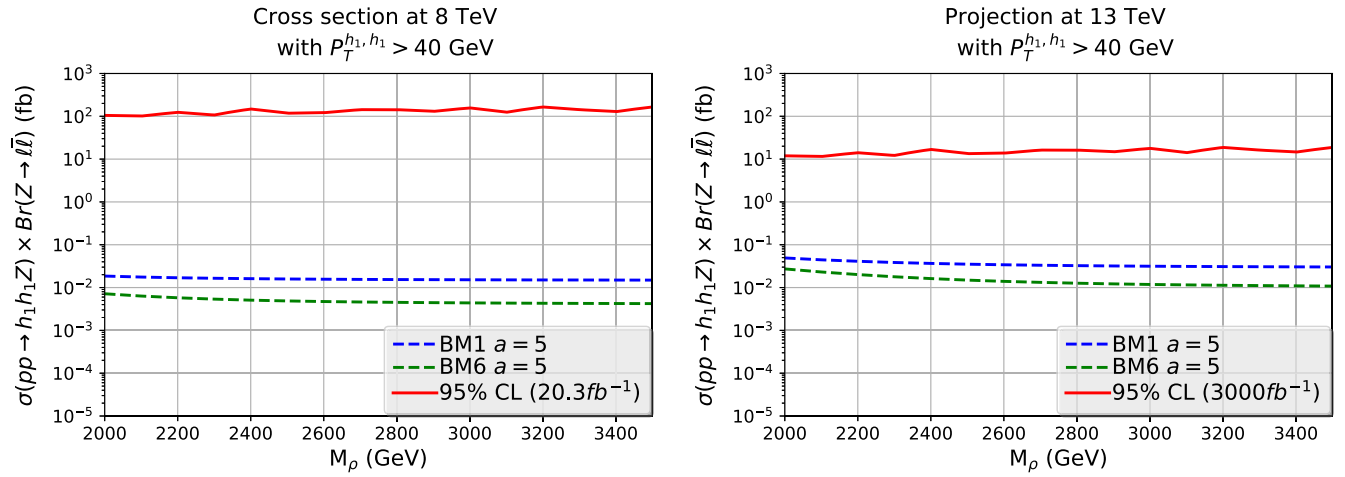

FIG. 10. $\sigma(pp \to h_1 h_1 Z)\mathrm{Br}(Z \to \ell\bar{\ell})$ vs M_ρ at Left: $\sqrt{s} = 8$ TeV and Right: $\sqrt{s} = 13$ TeV considering the benchmark points BM1 and BM6. The continuous line represent the minimum observable cross section at LHC.

However, the presence of the new heavy vector is not innocuous for the phenomenology of the dark matter candidate. In fact, it introduces new annihilation channels which are important in the region of large dark matter mass. The most important consequence of this phenomenon is the reduction of the relic density saturation zone compared with the usual i2DHM.

ACKNOWLEDGMENTS

This work was supported in part by Conicyt (Chile) Grants No. ACT1406 and PIA/Basal FB0821, and by Fondecyt (Chile) Grant No. 1160423. A. Z. is very thankful to the developers of MAXIMA [38] and the package Dirac2 [39]. These softwares were used in parts of this work.

[1] G. Aad *et al.* (ATLAS Collaboration), Observation of a new particle in the search for the standard model Higgs boson with the ATLAS detector at the LHC, Phys. Lett. B **716**, 1 (2012).
[2] S. Chatrchyan *et al.* (CMS Collaboration), Observation of a new boson at a mass of 125 GeV with the CMS experiment at the LHC, Phys. Lett. B **716**, 30 (2012).
[3] N. G. Deshpande and E. Ma, Pattern of symmetry breaking with two Higgs doublets, Phys. Rev. D **18**, 2574 (1978).
[4] L. Lopez Honorez, E. Nezri, J. F. Oliver, and M. H. Tytgat, The inert doublet model: An archetype for dark matter, J. Cosmol. Astropart. Phys. 02 (2007) 028.
[5] R. Barbieri, L. J. Hall, and V. S. Rychkov, Improved naturalness with a heavy Higgs: An Alternative road to LHC physics, Phys. Rev. D **74**, 015007 (2006).
[6] M. A. Luty, Dynamical electroweak symmetry breaking with two composite Higgs doublets, Phys. Rev. D **41**, 2893 (1990).
[7] J. Mrazek, A. Pomarol, R. Rattazzi, M. Redi, J. Serra, and A. Wulzer, The other natural two Higgs doublet model, Nucl. Phys. **B853**, 1 (2011).
[8] E. Bertuzzo, T. S. Ray, H. de Sandes, and C. A. Savoy, On composite two Higgs doublet models, J. High Energy Phys. 05 (2013) 153.
[9] S. De Curtis, S. Moretti, K. Yagyu, and E. Yildirim, LHC Phenomenology of composite 2-Higgs doublet models, Eur. Phys. J. C **77**, 513 (2017).
[10] S. De Curtis, S. Moretti, K. Yagyu, and E. Yildirim, Theory and phenomenology of composite 2-Higgs doublet models, *Proc. Sci.*, CHARGED2016 (2016) 018 [arXiv:1612.05125].
[11] S. Di Chiara, M. Heikinheimo, and K. Tuominen, Vector resonances at LHC Run II in composite 2HDM, J. High Energy Phys. 03 (2017) 009.
[12] S. De Curtis, S. Moretti, K. Yagyu, and E. Yildirim, Perturbative unitarity bounds in composite two-Higgs doublet models, Phys. Rev. D **94**, 055017 (2016).
[13] A. R. Zerwekh, Two composite Higgs doublets: Is it the low energy limit of a natural strong electroweak symmetry breaking sector?, Mod. Phys. Lett. A **25**, 423 (2010).
[14] M. Bando, T. Kugo, S. Uehara, K. Yamawaki, and T. Yanagida, Is the ρ Meson a Dynamical Gauge Boson of Hidden Local Symmetry?, Phys. Rev. Lett. **54**, 1215 (1985).
[15] G. C. Branco, P. M. Ferreira, L. Lavoura, M. N. Rebelo, M. Sher, and J. P. Silva, Theory and phenomenology of two-Higgs-doublet models, Phys. Rep. **516**, 1 (2012).
[16] F. Staub, Reopen parameter regions in two-Higgs doublet models, arXiv:1705.03677.
[17] I. F. Ginzburg, K. A. Kanishev, M. Krawczyk, and D. Sokolowska, Evolution of Universe to the present inert phase, Phys. Rev. D **82**, 123533 (2010).
[18] A. Arhrib, R. Benbrik, and N. Gaur, $H \to \gamma\gamma$ in inert Higgs doublet model, Phys. Rev. D **85**, 095021 (2012).
[19] A. Belyaev, G. Cacciapaglia, I. P. Ivanov, F. Rojas, and M. Thomas, Anatomy of the inert two Higgs doublet model in the light of the LHC and non-LHC dark matter searches, arXiv:1612.00511.
[20] M. Baak, J. Cuth, J. Haller, A. Hoecker, R. Kogler, K. Munig, M. Schott, and J. Stelzer (Gfitter Group Collaboration), The global electroweak fit at NNLO and prospects for the LHC and ILC, Eur. Phys. J. C **74**, 3046 (2014).
[21] R. S. Chivukula, E. H. Simmons, H.-J. He, M. Kurachi, and M. Tanabashi, Electroweak corrections and unitarity in linear moose models, Phys. Rev. D **71**, 035007 (2005).
[22] A. E. C. Hernandez, C. O. Dib, and A. R. Zerwekh, The effect of composite resonances on Higgs decay into two photons, Eur. Phys. J. C **74**, 2822 (2014).
[23] A. E. C. Hernandez, B. D. Saez, C. O. Dib, and A. Zerwekh, Constraints on vector resonances from a strong Higgs sector, arXiv:1707.05195.
[24] O. Castillo-Felisola, C. Corral, M. González, G. Moreno, N. A. Neill, F. Rojas, J. Zamora, and A. R. Zerwekh, Higgs boson phenomenology in a simple model with vector resonances, Eur. Phys. J. C **73**, 2669 (2013).
[25] M. Gintner and J. Juran, The LHC mass limits for the $SU(2)_{L+R}$ vector resonance triplet of a strong extension of the standard model, Acta Phys. Pol. B **48**, 1383 (2017).
[26] ATLAS Collaboration, ATLAS-CONF-2016-069, 2016.
[27] G. Aad *et al.* (ATLAS and C. Collaborations), Measurements of the Higgs boson production and decay rates and constraints on its couplings from a combined ATLAS and CMS analysis of the LHC pp collision data at $\sqrt{s} = 7$ and 8 TeV, J. High Energy Phys. 08 (2016) 045.
[28] G. Aad *et al.* (ATLAS Collaboration), Search for invisible decays of a Higgs boson using vector-boson fusion in pp collisions at $\sqrt{s} = 8$ TeV with the ATLAS detector, J. High Energy Phys. 01 (2016) 172.
[29] CMS Collaboration, CERN Report No. CMS-PAS-HIG-15-012, 2015 https://cds.cern.ch/record/2054465.
[30] G. Belanger, F. Boudjema, A. Pukhov, and A. Semenov, micrOMEGAs_3: A program for calculating dark matter observables, Comput. Phys. Commun. **185**, 960 (2014).

[31] G. Belanger, F. Boudjema, A. Pukhov, and A. Semenov, MicrOMEGAs 2.0: A program to calculate the relic density of dark matter in a generic model, Comput. Phys. Commun. **176**, 367 (2007).

[32] G. Belanger, F. Boudjema, P. Brun, A. Pukhov, S. Rosier-Lees, P. Salati, and A. Semenov, Indirect search for dark matter with micrOMEGAs2.4, Comput. Phys. Commun. **182**, 842 (2011).

[33] A. Belyaev, N. D. Christensen, and A. Pukhov, CalcHEP 3.4 for collider physics within and beyond the standard model, Comput. Phys. Commun. **184**, 1729 (2013).

[34] P. A. R. Ade *et al.* (Planck Collaboration), Planck 2013 results. XVI. Cosmological parameters, Astron. Astrophys. **571**, A16 (2014).

[35] P. Ade *et al.* (Planck Collaboration), Planck 2015 results. XIII. Cosmological parameters, Astron. Astrophys. **594**, A13 (2016).

[36] E. Aprile *et al.* (XENON Collaboration), First Dark Matter Search Results from the XENON1T Experiment, Phys. Rev. Lett. **119**, 181301 (2017).

[37] M. Drees, H. Dreiner, D. Schmeier, J. Tattersall, and J. S. Kim, CheckMATE: Confronting your favourite new physics model with LHC data, Comput. Phys. Commun. **187**, 227 (2015).

[38] Maxima, Maxima, a computer algebra system. version 5.40.0, 2017. http://maxima.sourceforge.net/.

[39] E. L. Woollett, Dirac2: A high energy physics package for maxima, 2012. http://web.csulb.edu/woollett/.